Journal of Sound and Vibration 326 (2009) 88–103

Contents lists available at ScienceDirect

Journal of Sound and Vibration

journal homepage: www.elsevier.com/locate/jsvi

Theoretical design parameters for a quasi-zero stiffness magnetic spring for vibration isolation

Will S. Robertson *, M.R.F. Kidner, Ben S. Cazzolato, Anthony C. Zander

School of Mechanical Engineering, University of Adelaide, Australia

ARTICLE INFO

Article history:
Received 6 May 2008
Received in revised form
9 April 2009
Accepted 10 April 2009
Handling Editor: L.G. Tham
Available online 23 May 2009

ABSTRACT

This paper presents an analysis of a magnetic levitation system for vibration isolation. A non-dimensional analysis of the magnetic support is considered and it is shown analytically that for cubical magnets the ratio of force to displacement is directly proportional to face area. The arrangement of magnets examined uses a negative stiffness element to reduce the natural frequency of the suspension. Design criteria are imposed on the system to satisfy mass loading, bandwidth of the required isolation, expected magnitude of the vibration disturbance and required robustness of the system. The vibration response of a system designed to satisfy these requirements is compared to an equivalent linear system and is shown to become increasingly nonlinear as the system moves towards instability.

1. Motivation

The main mechanisms of vibration isolation have been researched in detail and are now well known [1]. For a single degree of freedom system, reducing the stiffness has the effect of lowering the resonance frequency, while increasing the damping reduces the amplitude of the resonance peak to the detriment of isolation at higher frequencies. These adjustments can be made by modifying the physical structure or by applying displacement or relative velocity active feedback control.

Absolute velocity feedback control creates 'sky-hook' damping, in which the resonance peak is reduced without affecting the vibration transmission at higher frequencies [2]. For an ideal single degree of freedom system, this technique is limited by instability caused by time delays in the controller [3,4].

Semi-active methods have also been developed to approximate this technique when fully active control is undesirable [5–7]. Semi-active control has the advantages of robustness and low power requirements, especially when large forces would be required for active control.

Reducing the stiffness of the support decreases the resonance frequency of the system, which increases the bandwidth of vibration isolation. This will improve the vibration isolation of the system over the application of sky-hook damping, especially at low frequencies. For a given mass, this can be achieved by reducing the stiffness of the support, or by adding a negative stiffness element in parallel with the system [8,9]. Again, this can be implemented by passive, active or semi-active methods. Negative displacement or positive acceleration feedback can be used in a fully active system. In the semi-active case, many methods exist to dynamically adjust the stiffness depending on the support being used; an example has been demonstrated by Kidner and Brennan [10].

* Corresponding author.
E-mail address: will@mecheng.adelaide.edu.au (W.S. Robertson).

0022-460X/$ - see front matter © 2009 Elsevier Ltd. All rights reserved.
doi:10.1016/j.jsv.2009.04.015

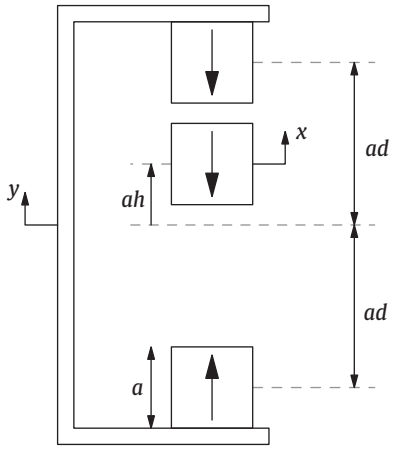

Fig. 1. Schematic of a magnetic spring with quasi-zero stiffness at $h = 0$ to isolate displacement x from disturbance vibration y. Large arrows indicate direction of polarisation of the magnets. In this paper, cubical magnets are used with side length a, distance $2ad$ between the centres of the fixed magnets, and displacement of the floating magnet from the zero stiffness position ah. Position shown at positive h (upwards) corresponds to unstable equilibrium; negative h (downwards) is stable.

In a conventional mass–spring system, the static deflection increases as the stiffness of the support is reduced, and a lower limit on the stiffness is imposed by constraints on the allowable displacement. Less typical supports can exhibit stiffness that varies nonlinearly with displacement; even local regions of zero stiffness are possible. An example of a system with such a behaviour is a parallel connection of vertical and inclined springs [11–14], which has an approximately cubic force vs. displacement characteristic; localised zero stiffness occurs at zero deflection, which is termed 'quasi-zero stiffness'. The use of buckling beams as a negative stiffness element to achieve quasi-zero stiffness has also been implemented in practice [15,16]. An example pertinent to this research is the recent analysis by Carrella et al. [17] of a quasi-zero stiffness system using (positive stiffness) linear springs in parallel with negative stiffness magnetic springs. Further detail into the field of nonlinear passive vibration isolators is given in the recent review by Ibrahim [18].

This paper examines another system that exhibits localised zero stiffness: a pair of fixed magnets that supports a mass against gravity by, respectively, repelling the mass from below and attracting it from above, as shown in Fig. 1. This arrangement of magnets has seen some previous attention [19–21]. The force vs. displacement characteristic for this system has previously been approximated by a quadratic polynomial, valid only for small variations in the gaps between the magnets.

The cubic force curve is more useful because it creates a stable inflection point with localised zero stiffness; in contrast, a quadratic-type spring is marginally stable at its quasi-zero stiffness position and cannot be operated about this point. Nonetheless, the magnet arrangement is worth studying as a mechanism to achieve *low* stiffness, since this device reduces the stiffness in all three translational degrees of freedom. As well as its use to design low frequency isolation mounts, this idea can have particular application in support structures where a reduction in stiffness is desired to mitigate a vibration problem that has been discovered after its construction. The non-contact nature of the force between the magnets allows their easy attachment to an existing structure.

The structure of this paper is as follows. The exact equation for the forces between two cubical magnets is presented in Section 2 and used to calculate the exact and approximate force vs. displacement profiles of the quasi-zero stiffness magnetic spring. In Section 3, the criteria that govern the behaviour of a vibration isolation device are applied to the magnetic spring and suitable ranges for the design parameters are found to achieve the design goals. Finally, Section 5 analyses the dynamic behaviour of the spring to ensure that the isolation capabilities are not compromised by the nonlinear characteristics of the magnetic spring.

2. Magnet forces

The force that is generated between parallel cuboid magnets (i.e., with faces orthogonal but not necessarily equal) can be calculated with the formulation of Akoun and Yonnet [22], for magnet geometries depicted in Fig. 2. Bancel [23] published an equivalent equation that is algorithmically easier to apply for complex magnet geometries and multipole arrays.

For this work, the original expression of Akoun and Yonnet [22] is simplified for cubical magnets with a vertical offset; i.e., magnet sizes $a = b = c = A = B = C$ and only vertical relative displacements, such that $\alpha = \beta = 0$. The distance between the magnet centres with respect to the size of the magnets is expressed as a normalised length:

$$l = \gamma/a. \tag{1}$$

After some manipulation of the original equation given these simplifying assumptions, the force $F_m(a, l)$ on the second magnet in attraction (i.e., for magnets with polarisation in the same direction) can be shown to be directly proportional to

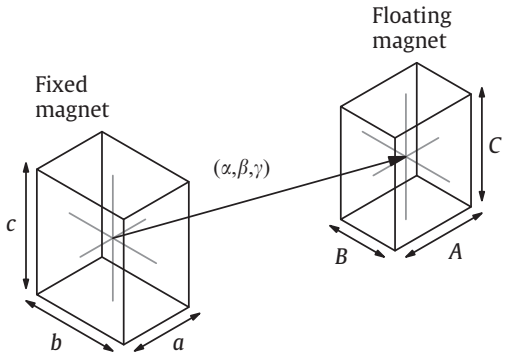

Fig. 2. Geometry for the expression by Akoun and Yonnet [22] to calculate the forces between two parallel cuboid magnets with magnetisations in the vertical direction, distance between their centres (α, β, γ), and magnet sizes as shown.

the facing area of the magnets, a^2, for a fixed normalised displacement, l, between the magnets:

$$F_m(a,l) = a^2 f_m(l). \tag{2}$$

For magnets in repulsion, the expression has opposite sign. The derived expression for the normalised force $f_m(l)$ is given in Eq. (A.1) in the appendix. The a^2 relationship shown in Eq. (2) is interesting because it is not evident from Akoun and Yonnet's original equations that such a simplification (for various subsets of magnet geometries such as the one considered here) is possible.

The stiffness between two cubical magnets can be calculated by differentiating the force expression in Eq. (2) with respect to vertical displacement $\gamma = al$ and can be shown to be proportional to the magnet size a:

$$K_m(a,l) = \frac{\partial}{\partial \gamma} F_m(a,l) = \frac{1}{a}\frac{\partial}{\partial l} a^2 f_m(l) = a k_m(l). \tag{3}$$

The derived expression for the normalised stiffness $k_m(l)$ is given in Eq. (A.3) in the Appendix.

A 'quasi-zero stiffness' magnetic spring consists of an attracting magnetic pair above a repelling magnet pair as shown in Fig. 1. Parameter ad is the gap between the centres of the magnet pairs at quasi-zero stiffness, and $x = ah$ is the static displacement of the floating mass about the centre line between the magnets. The parameters d and h are referred to as the normalised magnet gap and the normalised magnet displacement, respectively. The force due to the lower magnet in repulsion is

$$F_{\text{repl}}(a,d,h) = -F_m(a, ad + ah) \tag{4}$$

$$= -a^2 f_m(d+h), \tag{5}$$

and the force due to the upper magnet in attraction is

$$F_{\text{attr}}(a,d,h) = F_m(a, -ad + ah) \tag{6}$$

$$= a^2 f_m(-d+h). \tag{7}$$

The total force on the floating magnet, $F_z(a,d,h)$, is a superposition of $F_{\text{repl}}(a,d,h)$ and $F_{\text{attr}}(a,d,h)$, yielding

$$F_z(a,d,h) = F_{\text{repl}}(a,d,h) + F_{\text{attr}}(a,d,h) \tag{8}$$

$$= a^2\left[-f_m(d+h) + f_m(-d+h)\right] \tag{9}$$

$$\stackrel{\text{def}}{=} a^2 f_z(d,h). \tag{10}$$

The stiffness of the system can be similarly expressed as

$$K_z(a,d,h) = a k_z(d,h), \tag{11}$$

where

$$k_z(d,h) = -k_m(d+h) + k_m(-d+h). \tag{12}$$

The force $f_z(d,h)$ and stiffness $k_z(d,h)$ of the magnetic spring are readily calculated for values of normalised displacement and gap, h and d, from the derived expressions in the appendix. However, these expressions are too complex for use in any calculation where they must be inverted (say, finding a value of d for which a certain $k_z(d,h)$ holds). It is therefore necessary to obtain a simpler model of $f_z(d,h)$.

Previously, $f_z(d,h)$ has been modelled as a quadratic polynomial [19,20] with coefficients that vary with magnet gap:

$$f_z(d,h) \approx q_2(d)h^2 + q_0(d). \tag{13}$$

Over small displacement ranges this approximation yields adequate results, but the resulting model is dependent on the gap between the magnets and local to the displacement range used to fit the model.

A more accurate result (which is also accurate over larger displacement ranges) can be achieved with a quartic polynomial approximation,

$$f_z(d,h) \approx c_4(d)h^4 + c_2(d)h^2 + c_0(d), \tag{14}$$

but the same criticisms hold as for the quadratic polynomial model: the resulting model is not general; furthermore, if the model approximation is to also represent changes in magnet gap d, the functions $c_0(d)$, $c_2(d)$, and $c_4(d)$ require high-order polynomials to represent the variation sufficiently well.

Due to the complexity of the expression, a simpler approximation of the normalised force $f_m(l)$ can be found by fitting the constant coefficients A, B, and possibly n in the empirical approximation for the forces between two magnets

$$f_m(l) \approx \frac{A}{[B+l]^n}. \tag{15}$$

Xu and Tamura [24] used the more complicated approximation

$$f_m(l) \approx D\left[\frac{A}{B+l}\right]^n + C, \tag{16}$$

although in this case the additional complexity does not justify the slight increase in accuracy this expression may offer.

Bonisoli and Vigliani [25,26] used $n = 3$ in their work, and Piombo et al. [27] recommended either $n = 2$ or 4. The values for n they selected were based on the best fit curves of the forces for the specific geometry of their magnets in each case. However, n is not restricted to integer values and does not have to be chosen *a priori* to the curve fitting.

A least squares fit is performed with Eq. (15) varying all three parameters A, B, and n over the range $2 \leqslant h \leqslant 5$ to achieve an approximation of Eq. (A.1). Over the displacement range used to fit the model, modelling errors of less than 1% are achieved. (Without loss of generality, the magnetisation of each magnet, J, is taken as unity.) Including displacements outside of this range (especially $1 < h \leqslant 2$) diminishes the accuracy of the fit, but is less relevant for this work: displacements $1 < h \leqslant 2$ generate high stiffnesses, and displacements $h \geqslant 5$ have low supporting forces. Both of these properties are undesirable for a vibration isolator in terms of resonance frequency and adequate load bearing, respectively.

Fig. 3 shows the approximations found with Eq. (15) for set values $n = 3$ and 4 (only coefficients A and B are varied); in the third curve, n has also been allowed to range for the least-squared fit. Table 1 displays the values for all three calculated parameters in each case. The curves for $n = 2$ and $n = 5$ produce much greater errors than those shown in Fig. 3 and have been omitted for clarity.

An empirical approximation of Eq. (2) for the force between two cubical magnets is thus given by

$$F_m(a,x) \approx \pm a^2 J^2 \frac{6.028 \times 10^5}{[0.1883 + x]^{4.197}} \tag{17}$$

with force $F_m(a,x)$ in Newtons, magnet size a and displacement x both in metres, and magnetisation J in Tesla, where the expression is positive for magnets in repulsion and negative for magnets in attraction.

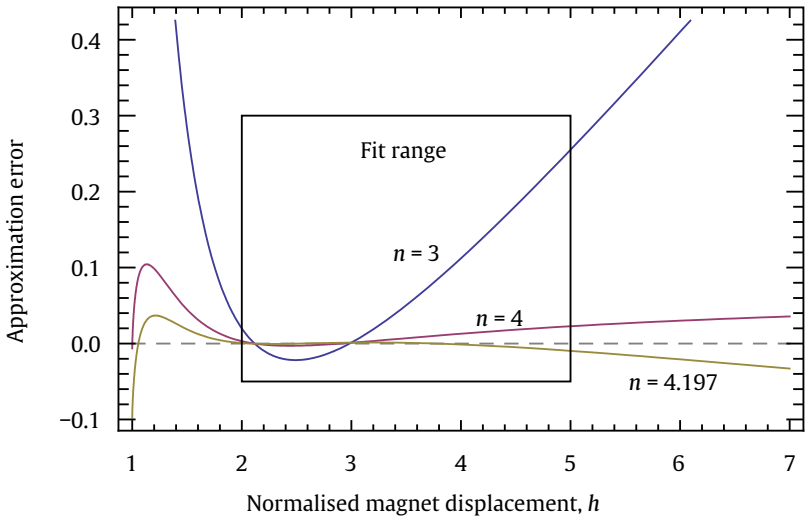

Fig. 3. Modelling errors of Eq. (15) compared to the exact Eq. (A.1), for parameters shown in Table 1.

Table 1
Best fit parameters for Eq. (15).

n	A	B
3	6.580×10^4	−0.5796
4	4.071×10^5	0.0607
4.197	6.028×10^5	0.1883

Note that these are unitless parameters. Fixed integer values of n were chosen for the first two cases, and the latter value best fits the model by varying all three parameters.

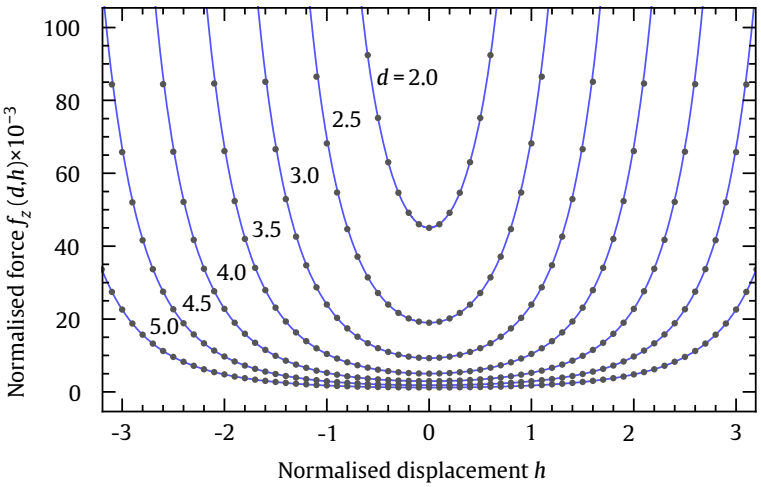

Fig. 4. Normalised force $f_z(d,h)$ vs. displacement h curves of a quasi-zero stiffness magnetic system for a range of normalised gap d (the stiffness is zero at $h=0$). Single points correspond to the exact solution; solid lines correspond to the approximation given by Eq. (15).

Fig. 4 shows the model of the magnetic system using Eq. (15) to calculate the force due to the repelling and attracting magnets separately:

$$f_z(d,h) \approx A[B+d+h]^{-n} + A[B+d-h]^{-n}, \tag{18}$$

where A, B, and n are the best-fit parameters previously discussed. This solution is both simpler in form and more accurate than the polynomial models of Eqs. (13) and (14). It is also much easier to invert numerically than the exact Eq. (10), although note that Eq. (18) still cannot be algebraically inverted; this is not an issue for the work to be discussed in the following sections. The normalised stiffness can be approximated by differentiating Eq. (18) with respect to h: (as shown previously in Eq. (3))

$$k_z(d,h) \approx nA[B+d+h]^{-n-1} + nA[B+d-h]^{-n-1}. \tag{19}$$

In this section, a model of the magnet forces was presented that is accurate over large relative displacements. Despite the fact that the vibration disturbance will occur in small magnitudes relative to the size of the magnet dimension, it is important to model the magnet forces accurately over a large displacement range so that the design evaluations in the next section may be applied over variations in magnet gap.

3. Design criteria

In the previous section, a magnetic system was introduced with an exact expression and various approximations for calculating the force vs. displacement characteristics for a range of system designs. It is proposed that this system is suitable for a vibration isolation platform due to the possibility of low inherent stiffness of the design. However, the stiffness is dependent on the load that is being supported, and the magnetic arrangement must be designed for this purpose. In this section, constraints are imposed on the system parameters to satisfy these criteria and a design principle developed.

The normalised equilibrium position of the system h_q can be found by equating the magnet force at equilibrium f_q with the load due to gravity and inverting numerically:

$$f_q(a,d,M) = f_z(d,h_q) = Mg/a^2. \tag{20}$$

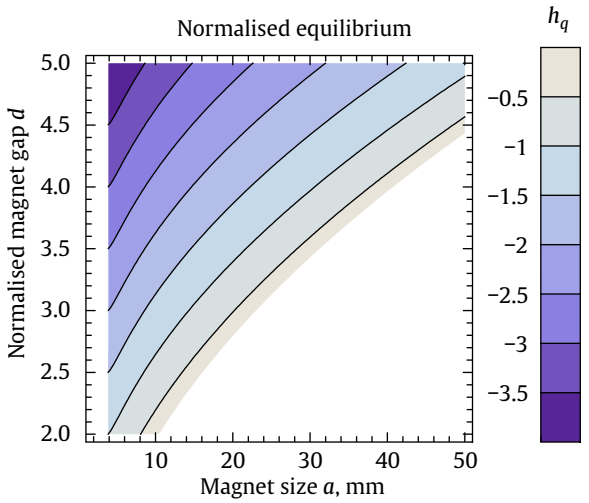

Fig. 5. Map of the normalised equilibrium position over varying magnet size a and normalised magnet gap d for a system with mass $M = 0.5$ kg.

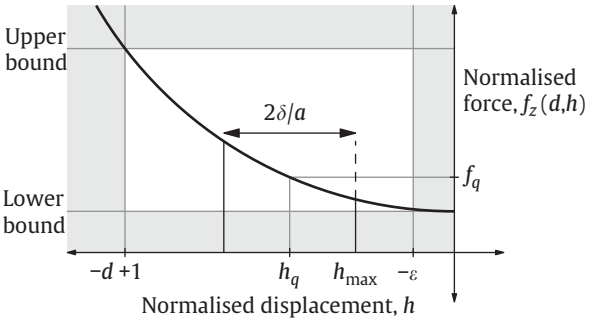

Fig. 6. Normalised force vs. normalised displacement curve illustrating the bounds of both allowable load that can be borne and the displacement range of the magnet; see Eqs. (21) and (24), respectively, for the mathematical representations. $-d+1$ is the position where the floating magnet is touching the upper face of the lower fixed magnet, and $-\varepsilon$ is the closest allowable position to the quasi-zero stiffness position.

A positive displacement of the mass ($h \geqslant 0$) is unstable, and so Eq. (20) must be solved such that $h_q < 0$. Fig. 5 shows the equilibrium position h_q varying over a and d for a system of mass $M = 0.5$ kg.

The normalised equilibrium position h_q of a mass can be approximated from the polynomial fits of the force curve by equating, for example, Eq. (14) with the force due to gravity and solving for h. However, the more accurate approximation Eq. (18) cannot be algebraically rearranged to solve for h; hence, solutions based on that equation must be obtained numerically.

The magnet size and gap must be chosen based on h_q to ensure that the spring is of sufficient stiffness to support a desired load but not so strong that the supported mass cannot be in equilibrium in the stable region of the spring. A 'static deflection criterion' is defined to achieve these constraints:

$$f_z(d,0) < Mg/a^2 < f_z(d,-d+1), \tag{21}$$

which is shown graphically in Fig. 6. This criterion is depicted in Fig. 7 as a region over the parameters a and d for three mass loads. The shape and location of the regions show that for a fixed magnet gap, larger magnets are required to support larger loads.

Assuming that linearisation is appropriate to model the vibration response of the system, the equivalent linear stiffness at equilibrium, K_q, must satisfy the resonance frequency criterion: $K_q = K_z(a,d,h_q) \leqslant \omega_d^2 M$, where ω_d is the maximum allowable resonance frequency. From Eq. (19), this requirement can be formulated as

$$[B+d+h_q]^{-n-1} + [B+d-h_q]^{-n-1} \leqslant \frac{\omega_d^2 M}{anA}. \tag{22}$$

This criterion is shown in Fig. 8 for a range of desired nominal stiffnesses. As the resonance frequency decreases, larger magnets are required to support the load with a small force gradient.

Finally, the amplitude of the input vibration must be smaller than the physical bounds of the system. This can be visualised on a normalised force/displacement plot as shown in Fig. 6. For a maximum (absolute) displacement, δ, of

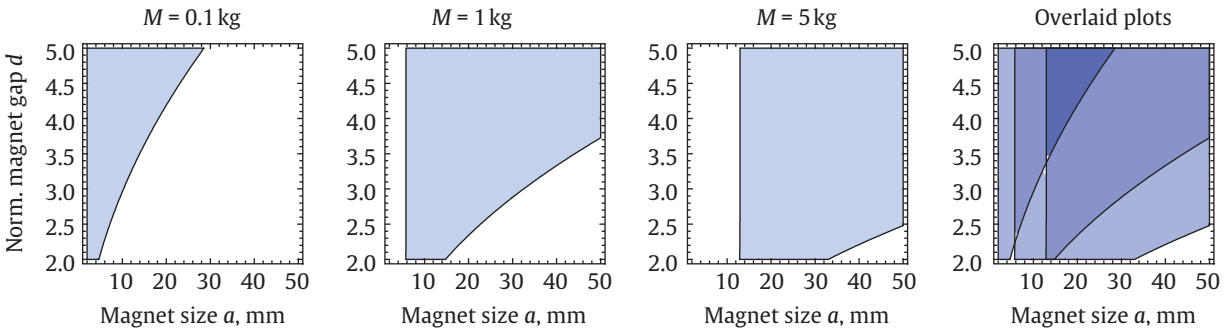

Fig. 7. Regions of a and d satisfying the static deflection criterion of Eq. (21) for a range of masses. Darker sections denote overlap of the regions in the overlay plot.

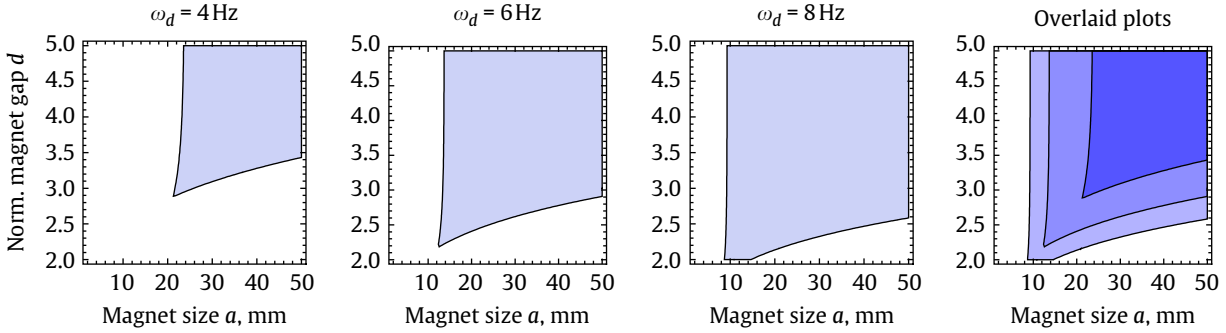

Fig. 8. Regions of a and d satisfying the resonance frequency criterion of Eq. (22) for a range of allowable resonance frequencies and a mass $M = 0.5$ kg. Darker sections denote overlap of the regions in the overlay plot.

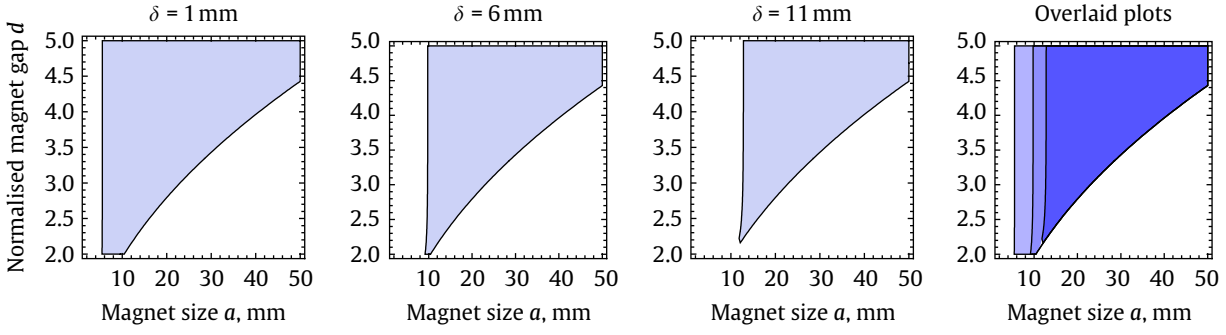

Fig. 9. Regions of a and h satisfying the maximum displacement criterion of Eq. (23) for a range of disturbance displacements δ and a mass $M = 0.5$ kg. Darker sections denote overlap of the regions in the overlay plot.

the mass,

$$h_q - \delta/a \geqslant -d + 1, \tag{23}$$

$$h_q + \delta/a < -\varepsilon, \tag{24}$$

where $a\varepsilon$ is the tolerance of the closest allowable distance to the (marginally stable) quasi-zero stiffness position that the system can operate. Eq. (23) is a maximum displacement criterion to ensure that the lower displacement bound lies above the face of the fixed lower magnet. Eq. (24) is a stability criterion to provide a buffer region to ensure that the moving magnet is not perturbed past the quasi-zero stiffness position into the unstable zone.

The latter constraints impose only small limits on the design of the system. The maximum displacement criterion, shown in Fig. 9 as a region over the parameters a and d for a range of δ, limits the lower size of the magnet.

Note that the maximum displacement of the spring will not be symmetric with input displacement due to the softening spring stiffness. Without loss of generality, however, it is possible to represent the maximum displacement in the stability and maximum displacement criteria (Eqs. (23) and (24)) with the same symbol.

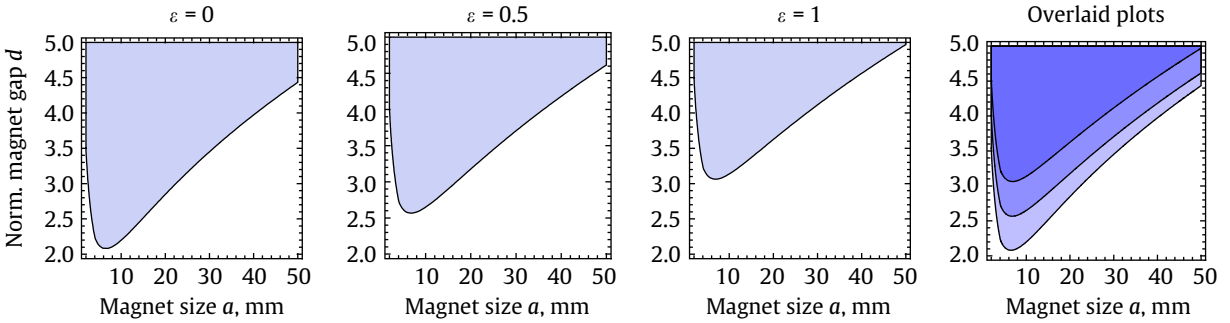

Fig. 10. Regions of a and d satisfying the stability criterion of Eq. (24) for a range of normalised displacement tolerances ε and a maximum disturbance displacement of $\delta = 5$ mm. Darker sections denote overlap of the regions in the overlay plot.

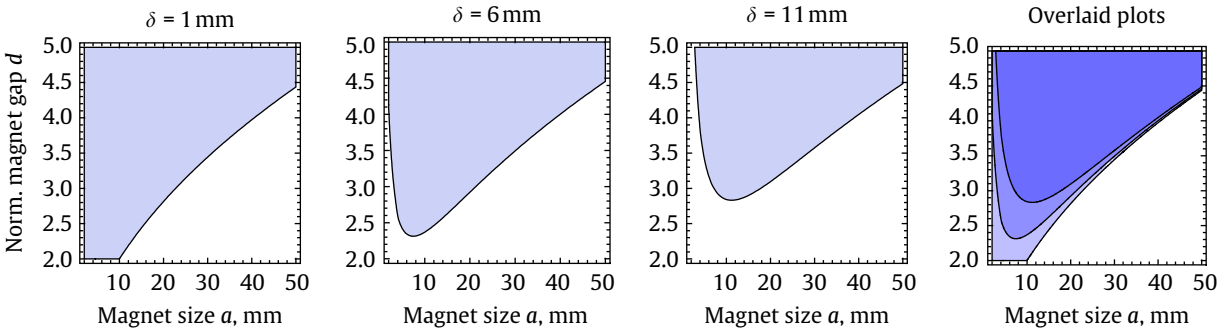

Fig. 11. Region of a, d satisfying the stability criterion of Eq. (24) for a range of disturbance displacements δ and a normalised displacement tolerance $\varepsilon = 0.1$. Darker sections denote overlap of the regions in the overlay plot.

The stability criterion is governed by two parameters, δ and ε, which are varied in Figs. 10 and 11, respectively. Again, this criterion only has a small effect on the constraint region, but it is an important effect. Because the stability criterion limits the minimum distance between the quasi-zero stiffness position and the equilibrium position, this prevents the spring from reaching the very low equilibrium stiffnesses found just below the quasi-zero stiffness position.

The introduced criteria may be simultaneously satisfied for some specified values of mass, resonance frequency, and displacement range (M, ω_d, and δ) by varying the free parameters magnet size a and magnet gap ad. The shared region of the criteria previously introduced (Eqs. (21)–(24)) are shown in Fig. 12 for various combinations of supported mass and resonance frequency. This figure presents a complete design map that shows how the techniques presented in this paper can be used for speculative design work and optimisation.

4. Measure of stiffness reduction

In the previous section, ranges for magnet size and magnet gap were shown to achieve certain design criteria. It is not impossible, however, that this process could yield a design that behaves acceptably with only a single repulsive magnet: the magnet gap could be so large as to render the effect of the negative stiffness negligible.

The total stiffness characteristic of the magnetic system is given by Eq. (12) as the sum of the stiffnesses due to repulsive and attractive magnets, respectively. At equilibrium, this can be written as

$$K_q(a,d,M) = K_{\text{repl}}(a,d,h_q) + K_{\text{attr}}(a,d,h_q) = K_{\text{repl}}[1-\kappa], \tag{25}$$

where

$$\kappa(a,d,h_q) = \left|\frac{K_{\text{attr}}}{K_{\text{repl}}}\right|. \tag{26}$$

The function $\kappa(a,d,h_q)$ can be considered as the ratio of 'stiffness reduction' achieved by the presence of the attractive magnet. For $\kappa = 0$, the upper magnet is providing no negative stiffness to the system; for $\kappa = 1$, the equilibrium position is at quasi-zero stiffness and the system is marginally stable.

Fig. 13 illustrates the variation of κ over a particular design region; this plot shows that designs achieved with larger magnet gaps have little influence from the stiffness reducing effect of the attractive magnet. As κ tends towards one, the

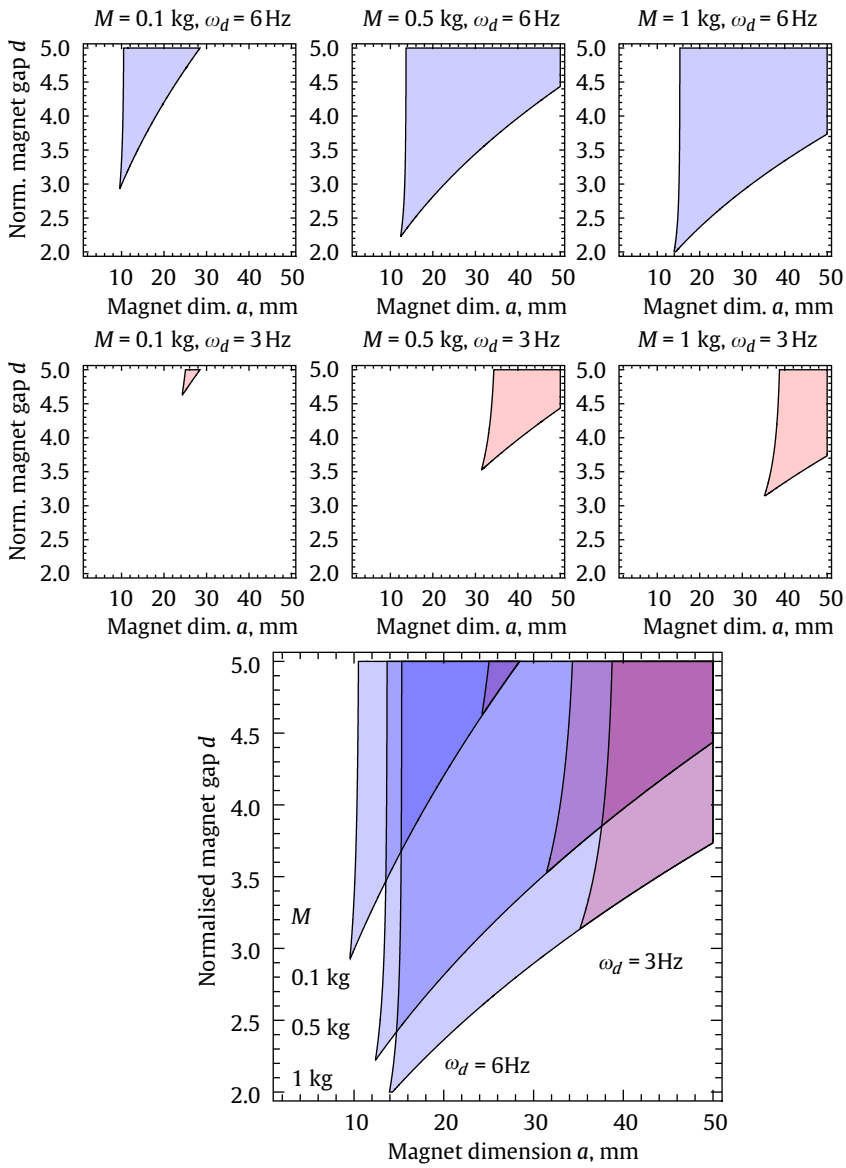

Fig. 12. Regions of a, d satisfying all design criteria, demonstrating the effects of changing the mass M and the resonance frequency ω_d of the desired system. Darker sections denote overlap of the regions in the overlay plot.

resonance frequency drops dramatically as the equilibrium position approaches the quasi-zero stiffness position (compare with Fig. 5).

5. Nonlinear behaviour

In Section 3, constraints were imposed on the design of the magnetic system such that a certain resonance frequency was achieved for a given mass loading. The slope of the force vs. displacement curve at equilibrium was used as the basis for the resonance frequency criterion. However, as the mass is perturbed from equilibrium the stiffness of the spring changes. When designing for vibration isolation, it is important to ensure that this nonlinearity does not produce a significant effect in the response of the system.

A measure of the nonlinearity of the system, η_k, can be found by comparing to the nominal stiffness the mean change in stiffness of the spring at equilibrium over its maximum peak-to-peak displacements from equilibrium:

$$\eta_k = \frac{\Delta K_z}{2K_q}, \tag{27}$$

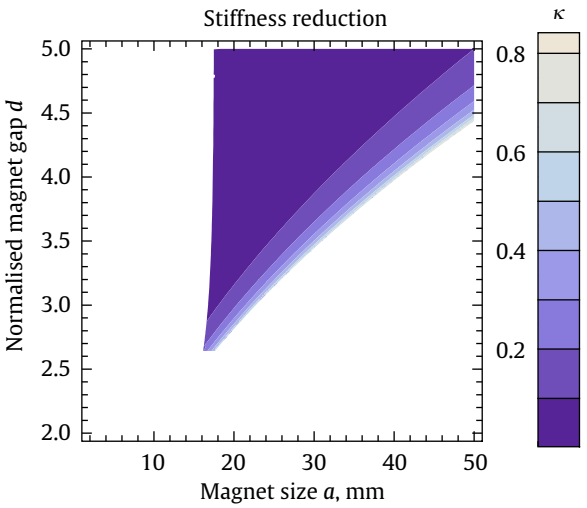

Fig. 13. Contours of stiffness reduction κ due to the negative stiffness of the attractive magnet, shown inside the region of a, d satisfying all design criteria for parameters $M = 1$ kg, $\omega_d = 5$ Hz, $\delta = 1$ mm, $\varepsilon = 0.1$.

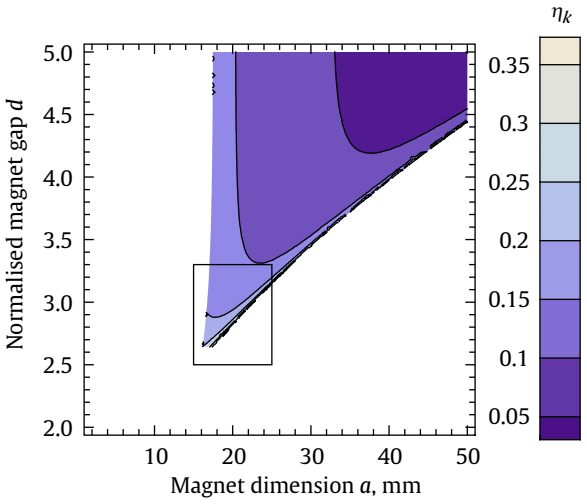

Fig. 14. Contours of nonlinearity shown inside the region of a, h satisfying all criteria for parameters $M = 1$ kg, $\omega_d = 5$ Hz, $\delta = 1$ mm, $\varepsilon = 0.1$. A closeup (of the box) is shown in Fig. 15.

where

$$\Delta K_z = K_z(a, d, h_q + \delta/a) - K_z(a, d, h_q - \delta/a), \tag{28}$$

$$K_q = K_z(a, d, h_q). \tag{29}$$

For the quadratic approximation of $f_z(d, h)$, η_k is a ratio between the maximum displacement and the equilibrium position:

$$\eta_k \approx \frac{\delta}{a h_q}, \tag{30}$$

and since $\delta/a < |h_q|$ for stability (recall Eq. (24)), it follows that the degree of nonlinearity is directly related to the amplitude of disturbance vibration. Fig. 14 demonstrates the manner in which η_k varies over an allowed region of design parameters, with $k_z(d, h)$ given by the exact expression of Eq. (12).

The nonlinearity measure increases both as magnet size and normalised magnet gap decrease. Comparing Fig. 14 to Figs. 5 and 13, it can also be seen that the nonlinearity measure increases the closer the equilibrium displacement becomes to the quasi-zero stiffness position, and the greater the effect of the negative stiffness from the attractive magnet (Fig. 15).

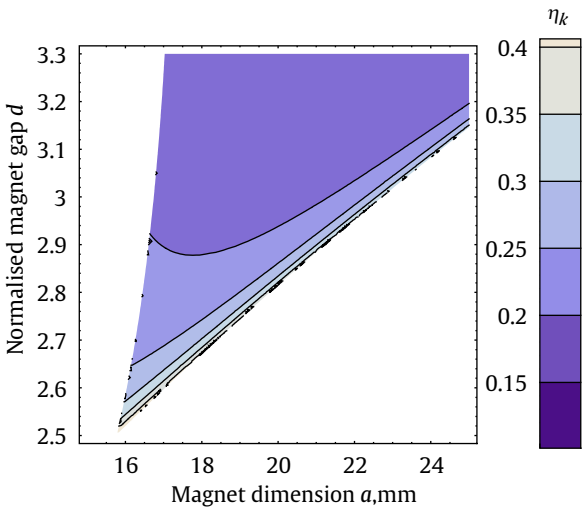

Fig. 15. Zoom of Fig. 14 to show the behaviour of the nonlinearity in the lower limits of the magnetic spring.

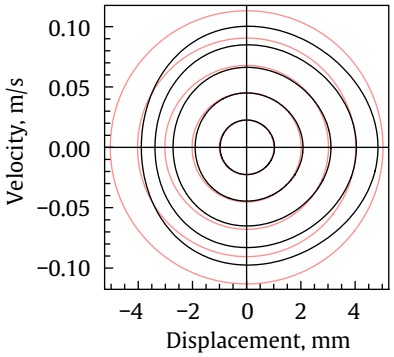

Fig. 16. Phase plot of the magnetic system at steady-state resonance for a range of input disturbance amplitudes shown in Table 2. The light line is the equivalent linear response.

Table 2
Nonlinearity values, η_k, of the responses shown in Fig. 16.

A_e, mm	ΔK_z, N/m	η_k
0.2	68	0.13
0.4	135	0.27
0.6	198	0.39
0.8	253	0.50
1.0	297	0.59

To analyse these nonlinear effects on the vibration response of the magnetic spring, the system shown in Fig. 1 is simulated with the dynamics

$$M\ddot{x} + b[\dot{x} - \dot{y}] - F_z(a, d, [x - y]/a) + Mg = 0, \tag{31}$$

where x is the displacement of the isolated mass and y is the displacement of the external disturbance. The system is excited tonally at resonance in order to depict the steady-state response with the greatest magnitude and therefore greatest nonlinearity. The excitation has amplitude A_e, and is given by

$$y = A_e \sin(\omega_n t). \tag{32}$$

The system parameters for the simulation are $M = 0.5$ kg, $a = 20$ mm, $d = 3$, excitation frequency $\omega_n = 3.58$ Hz, and equilibrium position h_q is 10.4 mm below the quasi-zero stiffness position. While the exact amount of damping present in

the system will be highly model-dependent, the damping coefficient is chosen as 5% based on the small damping forces due to eddy current and air resistance effects [19,28,29].

Fig. 16 shows the steady-state response of Eq. (31) for a range of ground disturbance amplitudes in even increments up to $A_e = 1$ mm. Because the excitation is at resonance, the output displacement is greater than the input displacement. The phase plot of the response becomes increasingly skewed as the amplitude of vibration, and hence the nonlinearity, increases; Table 2 summarises the nonlinearities calculated using Eq. (16). Physically, this is interpreted as the spring being perturbed further into the stiffer region as the mass is moved closer to the repulsive lower magnet, which results in stronger forces as the normalised displacement increases. Conversely, as the mass moves upwards, closer to the quasi-zero stiffness position, both the stiffness and the force decrease.

The results shown in Fig. 16 indicate that for small magnitude disturbances the phase plot is very similar to a linear system. As the amplitude increases, the nonlinear system response increases at a slower rate than the linear spring. This slowdown is due to a shifting of the resonance peak as the nonlinearity increases, as will be seen later in this section.

It is important to consider the role of damping in the results shown in Fig. 16. A low damping coefficient results in a greater resonance response in the low frequency range. This increase in the displacement response will also increase the nonlinear behaviour of the spring. However, the advantage of low damping is a very fast roll-off in vibration attenuation at frequencies above resonance. Since the damping of the non-contact magnetic spring is very low, either the bandwidth of excitation must lie above the resonance frequency or active sky-hook damping must be applied in order to reduce the strong effect that the resonance has on the low-frequency response. As previously discussed, sky-hook damping is especially suitable for this purpose because the isolation region of the frequency response is not affected.

5.1. Variance gain of the magnetic system

One metric to evaluate the response of a nonlinear system in the frequency domain is known as the 'variance gain' V [30], which is calculated as a ratio of the root-mean-square output to input signals:

$$V = \sqrt{\frac{1}{T}\int_0^T \bar{x}(t)^2\,\mathrm{d}t \Big/ \frac{1}{T}\int_0^T \bar{y}(t)^2\,\mathrm{d}t}, \tag{33}$$

where T is the time interval over which the variance gain is calculated, and $\bar{x}$ and $\bar{y}$ are the mean-zero output and input displacements of the vibration isolator, respectively. For linear systems, this expression simplifies to the standard formulation for transmissibility. For nonlinear systems, Eq. (33) describes the ratio of output to input energy for a given excitation. For the tonal input disturbance of Eq. (32), the variance gain at the frequency of excitation is

$$V = \frac{1}{A_e}\sqrt{\frac{2}{T}\int_0^T \bar{x}(t)^2\,\mathrm{d}t}. \tag{34}$$

The variance gain allows the nonlinearity of the system to be visualised on a familiar transmissibility-like plot for a range of resonant frequencies and equilibrium positions.

Fig. 17 shows the variance gain for a magnetic system with $M = 0.5$ kg, $a = 20$ mm, and $d = 2.8$ with excitation amplitude ranging from 0.1 mm to 0.5 mm. With these parameters, the equilibrium position is 1.55 mm below the

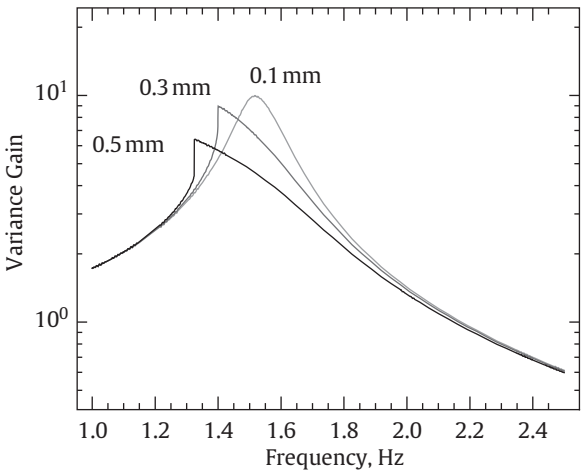

Fig. 17. Variance gain at a position close to quasi-zero stiffness, for a range of excitation amplitudes A_e, as labelled. The spring softening effect at resonance can be clearly seen as the amplitude increases. Tabulated values of nonlinearity and maximum displacement are shown in Table 3.

Table 3
Nonlinearity values, η_k, and maximum displacements, x_{max}, of the responses shown in Fig. 17.

A_e, mm	ΔK_z, N/m	x_{max}, mm	η_k
0.1	29.3	−1.04	0.31
0.3	57.6	−0.47	0.62
0.5	66.3	−0.24	0.71

The equilibrium stiffness is $K_q = 46.6$ N/m. The nonlinearity can be seen to increase with excitation amplitude. In the most extreme case, the magnetic system comes 0.24 mm from the quasi-zero stiffness position.

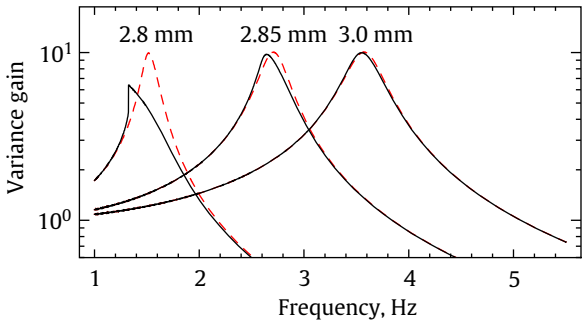

Fig. 18. Variance gain of the magnetic system, comparing between two excitation amplitudes with varying values of magnet gap d, as labelled. Low amplitude is $A_e = 0.1$ mm and high amplitude is $A_e = 0.5$ mm; shown as dashed and solid lines, respectively. The nonlinear effect is only prominent in the case close to quasi-zero stiffness, with an excitation amplitude that almost destabilises the system. Tabulated values of nonlinearity and maximum displacement are shown for the high amplitude case in Table 4.

Table 4
Nonlinearity values, η_k, and maximum displacements, x_{max}, of the high amplitude responses ($A_e = 0.5$ mm) shown in Fig. 4, for a range of magnet gaps, d.

d	K_q, N/m	ΔK_z, N/m	x_{max}, mm	η_k
2.8	66.3	46.6	−0.24	0.71
2.85	138.8	145.8	−2.72	0.48
3.0	167.6	253.5	−7.80	0.33

As the stiffness is decreased by the upper attractive magnet, greater nonlinearity is seen for smaller magnet gaps, as the equilibrium position moves closer to the point of quasi-zero stiffness .

quasi-zero stiffness position. As seen in the figure, the greater the excitation amplitude, the greater the softening nonlinearity of the spring.

Table 3 shows some data from the simulated responses, including the maximum displacement of the spring towards the quasi-zero stiffness position, and the nonlinearity measures η_k for each amplitude of excitation. The maximum displacement x_{max} corresponds with the maximum normalised displacement h_{max} shown in Fig. 6; as h_{max} tends towards zero, the motion of the magnetic spring moves closer to the quasi-zero stiffness position. Note that the pronounced nonlinearity seen in Fig. 17 belongs to a system that is approaching its bounds of stability, reaching 0.24 mm below the quasi-zero stiffness position in its most extreme displacement.

Fig. 18 shows the variance gain of the same system as the magnet gap d is increased. Results are shown for excitations of both $A_e = 0.1$ mm and $A_e = 0.5$ mm. Data for the simulations with $A_e = 0.5$ mm, including nonlinearity measure η_k and maximum displacement x_{max}, are shown in Table 4. Two related features are important to note from Fig. 18. The first is the large decrease in resonance frequency as the magnet gap decreases. The second is the corresponding increase in nonlinear behaviour as this occurs. As the equilibrium position moves away from the instability at quasi-zero stiffness, the variance gain quickly exhibits linear behaviour.

6. Summary

This paper has analysed a magnetic spring for the purposes of load bearing with low stiffness. Exact and approximate expressions were derived for cube-shaped magnets for analysing the behaviour of this system. The approximate expression is very simple and accurate over a large displacement range, and may be used for cubical magnets of any size.

Four design criteria were imposed on the system in terms of the two variable design parameters: magnet size and gap between the fixed magnets. A technique for explicitly mapping these constraints to a map of valid parameters was shown. Allowable stroke and magnet size availability allow a design to be optimised using this technique based on the required load bearing and resonance frequency.

The magnetic isolator is weakly nonlinear with a distorted phase plot compared to a linear system; the variance gain shows a resonance peak skewed into the lower frequencies. These nonlinearities only become apparent at larger vibration amplitudes at equilibrium positions that are close to the quasi-zero stiffness position (i.e., large measures of nonlinearity). Provided the system remains stable, the nonlinearities are not detrimental to the frequency response of the system.

The vibration isolator described in this paper is therefore suitable for precision applications where low resonance frequencies are required. The design is scalable in that many such isolators may be used in parallel to achieve greater load bearing even if only small magnets are available. The inherent low damping of the system results in good high frequency performance, but low frequency disturbances will result in large outputs due to the high resonance peak. This effect can be mitigated by the application of sky-hook damping to the system.

Appendix A. Analytical force and stiffness terms

The function $f_m(l)$ is the simplification of Akoun and Yonnet's [22] formula after the assumptions given in Section 2, where J_1 and J_2 are the magnetisations of the two magnets and $\mu_0 = 4\pi \times 10^{-7}$ is the 'permeability of the vacuum':

$$f_m(l) = \frac{J_1 J_2}{\pi \mu_0} \bar{f}_m(l), \tag{A.1}$$

where

$$\begin{aligned}
\bar{f}_m(l) = {} & [-2+l]\cdot|-2+l| - 2l|l| + [2+l]\cdot|2+l| + 4l\sqrt{4+l^2} \\
& - 2l\sqrt{8+l^2} + [4-2l]\sqrt{8-4l+l^2} + [-2+l]\sqrt{12-4l+l^2} \\
& + [-4-2l]\sqrt{8+4l+l^2} + [2+l]\sqrt{12+4l+l^2} \\
& + 2\left[4\arctan\left(\frac{4}{l\sqrt{8+l^2}}\right) + 2\arctan\left(\frac{4}{[2-l]\sqrt{12-4l+l^2}}\right)\right. \\
& -2\arctan\left(\frac{4}{[2+l]\sqrt{12+4l+l^2}}\right) + 2l\log\left(-2+\sqrt{4+l^2}\right) \\
& -2l\log\left(2+\sqrt{4+l^2}\right) - 2l\log\left(-2+\sqrt{8+l^2}\right) \\
& +2l\log\left(2+\sqrt{8+l^2}\right) + 2\log\left(-2+\sqrt{8-4l+l^2}\right) \\
& -l\log\left(-2+\sqrt{8-4l+l^2}\right) - 2\log\left(2+\sqrt{8-4l+l^2}\right) \\
& +l\log\left(2+\sqrt{8-4l+l^2}\right) - 2\log\left(-2+\sqrt{12-4l+l^2}\right) \\
& +l\log\left(-2+\sqrt{12-4l+l^2}\right) + 2\log\left(2+\sqrt{12-4l+l^2}\right) \\
& -l\log\left(2+\sqrt{12-4l+l^2}\right) - 2\log\left(-2+\sqrt{8+4l+l^2}\right) \\
& -l\log\left(-2+\sqrt{8+4l+l^2}\right) + 2\log\left(2+\sqrt{8+4l+l^2}\right) \\
& +l\log\left(2+\sqrt{8+4l+l^2}\right) + 2\log\left(-2+\sqrt{12+4l+l^2}\right) \\
& +l\log\left(-2+\sqrt{12+4l+l^2}\right) - 2\log\left(2+\sqrt{12+4l+l^2}\right) \\
& \left. -l\log\left(2+\sqrt{12+4l+l^2}\right)\right].
\end{aligned} \tag{A.2}$$

The normalised stiffness $k_m(l)$ is calculated by differentiating the force equations given by Akoun and Yonnet [22] before simplifying as with the force terms above:

$$k_m(l) = -\frac{2J_1J_2}{\pi\mu_0}\bar{k}_m(l), \tag{A.3}$$

where

$$\begin{aligned}\bar{k}_m(l) = {} & |-2+l| - 2|l| + |2+l| + 4\sqrt{4+l^2} - 2\sqrt{8+l^2} \\ & - 2\sqrt{8-4l+l^2} + \sqrt{12-4l+l^2} - 2\sqrt{8+4l+l^2} \\ & + \sqrt{12+4l+l^2} + 2\log(-2+\sqrt{4+l^2}) - 2\log(2+\sqrt{4+l^2}) \\ & - 2\log(-2+\sqrt{8+l^2}) + 2\log(2+\sqrt{8+l^2}) \\ & - \log(-2+\sqrt{8-4l+l^2}) + \log(2+\sqrt{8-4l+l^2}) \\ & + \log(-2+\sqrt{12-4l+l^2}) - \log(2+\sqrt{12-4l+l^2}) \\ & - \log(-2+\sqrt{8+4l+l^2}) + \log(2+\sqrt{8+4l+l^2}) \\ & + \log(-2+\sqrt{12+4l+l^2}) - \log(2+\sqrt{12+4l+l^2}).\end{aligned} \tag{A.4}$$

References

[1] C.R. Fuller, S.J. Elliot, P.A. Nelson, *Active Control of Vibration*, Academic Press, New York, 1996.

[2] B. Yan, M. Brennan, S. Elliott, N. Ferguson, Velocity feedback control of vibration isolation systems, ISVR Technical Memorandum 962, ISVR, March 2006 URL: ⟨http://www.isvr.soton.ac.uk/STAFF/Pubs/Pubpdfs/Pub8483.pdf⟩.

[3] S.J. Elliott, L. Benassi, M.J. Brennan, P. Gardonio, X. Huang, Mobility analysis of active isolation systems, *Journal of Sound and Vibration* 271 (1–2) (2004) 297–321 URL: ⟨http://dx.doi.org/10.1016/S0022-460X(03)00770-3⟩.

[4] M.J. Brennan, K.A. Ananthaganeshan, S.J. Elliott, Instabilities due to instrumentation phase-lead and phase-lag in the feedback control of a simple vibrating system, *Journal of Sound and Vibration* 304 (3–5) (2007) 466–478 URL: ⟨http://dx.doi.org/10.1016/j.jsv.2007.01.046⟩.

[5] Y. Liu, T. Waters, M. Brennan, B. Mace, Harmonic analysis of semi-active dampers, ISVR Technical Memorandum 900, University of Southampton, November 2002. URL: ⟨http://www.isvr.soton.ac.uk/STAFF/Pubs/Pubpdfs/Pub1608.pdf⟩.

[6] Y. Liu, T.P. Waters, M.J. Brennan, A comparison of semi-active damping control strategies for vibration isolation of harmonic disturbances, *Journal of Sound and Vibration* 280 (1–2) (2005) 21–39 URL: ⟨http://dx.doi.org/10.1016/j.jsv.2003.11.048⟩.

[7] M. Ahmadian, X. Song, S.C. Southward, No-jerk skyhook control methods for semiactive suspensions, *Journal of Vibration and Acoustics* 126 (4) (2004) 580–584 URL: ⟨http://dx.doi.org/10.1115/1.1805001⟩.

[8] C.-M. Lee, V. Goverdovskiy, A. Temnikov, Design of springs with 'negative' stiffness to improve vehicle driver vibration isolation, *Journal of Sound and Vibration* 302 (4–5) (2007) 865–874 URL: ⟨http://dx.doi.org/10.1016/j.jsv.2006.12.024⟩.

[9] J.T. Xing, Y.P. Xiong, W.G. Price, Passive–active vibration isolation systems to produce zero or infinite dynamic modulus: theoretical and conceptual design strategies, *Journal of Sound and Vibration* 286 (3) (2005) 615–636 URL: ⟨http://dx.doi.org/10.1016/j.jsv.2004.10.018⟩.

[10] M.R.F. Kidner, M.J. Brennan, Varying the stiffness of a beam-like neutralizer under fuzzy logic control, *Journal of Vibration and Acoustics* 124 (1) (2002) 90–99 URL: ⟨http://dx.doi.org/10.1115/1.1423634⟩.

[11] W.G. Molyneux, Supports for vibration isolation, ARC/CP-322, Aeronautical Research Council, Great Britain, 1957. URL: ⟨http://nsdl.org/resource/2200/20061003060308472T⟩.

[12] P. Alabuzhev, A. Gritchin, L. Kim, G. Migirenko, V. Chon, P. Stepanov, *Vibration Protecting and Measuring Systems with Quasi-Zero Stiffness, Applications of Vibration*, Hemisphere, Washington, DC, 1989.

[13] A. Carrella, T.P. Waters, M.J. Brennan, Optimisation of a passive vibration isolator with quasi-zero-stiffness characteristic, ISVR Technical Memorandum 960, University of Southhampton, February 2006. URL: ⟨http://www.isvr.soton.ac.uk/STAFF/Pubs/Pubpdfs/Pub8481.pdf⟩.

[14] A. Carrella, M.J. Brennan, T.P. Waters, Static analysis of a passive vibration isolator with quasi-zero-stiffness characteristic, *Journal of Sound and Vibration* 301 (3–5) (2007) 678–689 URL: ⟨http://dx.doi.org/10.1016/j.jsv.2006.10.011⟩.

[15] D.L. Platus, Negative-stiffness-mechanism vibration isolation systems, *Proceedings of SPIE—The International Society for Optical Engineering* 3786 (1999) 98–105 URL: ⟨http://dx.doi.org/10.1117/12.363841⟩.

[16] T. Tarnai, Zero stiffness elastic structures, *International Journal of Mechanical Sciences* 45 (3) (2003) 425–431 URL: ⟨http://dx.doi.org/10.1016/S0020-7403(03)00063-8⟩.

[17] A. Carrella, M.J. Brennan, T.P. Waters, K. Shin, On the design of a high-static-low-dynamic stiffness isolator using linear mechanical springs and magnets, *Journal of Sound and Vibration* 315 (3) (2008) 712–720 URL: ⟨http://dx.doi.org/10.1016/j.jsv.2008.01.046⟩.

[18] R.A. Ibrahim, Recent advances in nonlinear passive vibration isolators, *Journal of Sound and Vibration* 314 (3–5) (2008) 371–452 URL: ⟨http://dx.doi.org/10.1016/j.jsv.2008.01.014⟩.

[19] G.-J.P. Nijsse, Linear motion systems: a modular approach for improved straightness performance, PhD Thesis, Delft University of Technology, 2001. URL: ⟨http://repository.tudelft.nl/file/80827/161960⟩.

[20] W. Robertson, R. Wood, B. Cazzolato, A. Zander, Zero-stiffness magnetic springs for active vibration isolation, *Proceedings of the 6th International Symposium on Active Noise and Vibration Control*, 2006. URL: ⟨http://hdl.handle.net/2440/35429⟩.

[21] W.S. Robertson, B.S. Cazzolato, A.C. Zander, Nonlinear control of a one axis magnetic spring, *Proceedings of the 14th International Congress on Sound and Vibration*, Cairns, Australia, 2007. URL: ⟨http://hdl.handle.net/2440/44996⟩.

[22] G. Akoun, J.-P. Yonnet, 3D analytical calculation of the forces exerted between two cuboidal magnets, *IEEE Transactions on Magnetics* MAG-20 (5) (1984) 1962–1964 URL: ⟨http://ieeexplore.ieee.org/xpl/freeabs_all.jsp?arnumber=1063554⟩.

[23] F. Bancel, Magnetic nodes, *Journal of Physics D: Applied Physics* 32 (1999) 2155–2161 URL: ⟨http://dx.doi.org/10.1088/0022-3727/32/17/304⟩.

[24] Z. Xu, H. Tamura, Analyses of the chaotic vibration of a magnetically levitated body, *Memoirs of the Faculty of Engineering, Kyushu University* 53 (4) (1993) 209–233 URL: ⟨http://ci.nii.ac.jp/naid/110000020124/en/⟩.

[25] E. Bonisoli, A. Vigliani, Identification techniques applied to a passive elasto-magnetic suspension, *Mechanical Systems and Signal Processing* 21 (3) (2007) 1479–1488 URL: ⟨http://dx.doi.org/10.1016/j.ymssp.2006.05.009⟩.
[26] E. Bonisoli, A. Vigliani, Passive elasto-magnetic suspensions: nonlinear models and experimental outcomes, *Mechanics Research Communications* 34 (4) (2007) 385–394 URL: ⟨http://dx.doi.org/10.1016/j.mechrescom.2007.02.005⟩.
[27] B.A.D. Piombo, A. Vigliani, E. Bonisolo, Dynamics of suspensions with rare-earth permanent magnets, *Proceedings of the SPIE* 5052 (2003) 106–115.
[28] R.-F. Fung, Y.-T. Liu, C.-C. Wang, Dynamic model of an electromagnetic actuator for vibration control of a cantilever beam with a tip mass, *Journal of Sound and Vibration* 288 (4–5) (2005) 957–980 URL: ⟨http://dx.doi.org/j.jsv.2005.01.046⟩.
[29] E. Bonisoli, A. Vigliani, Passive effects of rare-earth permanent magnets on flexible conductive structures, *Mechanics Research Communications* 33 (3) (2006) 302–319 URL: ⟨http://dx.doi.org/10.1016/j.mechrescom.2005.08.011⟩.
[30] S.M. Savaresi, C. Spelta, Mixed sky-hook and ADD: approaching the filtering limits of a semi-active suspension, *Journal of Dynamic Systems, Measurement, and Control* 129 (4) (2007) 382–392 URL: ⟨http://dx.doi.org/10.1115/1.2745846⟩.